Uniosun Journal of Engineering and Environmental Sciences (UJEES), Vol. 8 No. 2, Sept., 2026
DOI: 10.64980/ujees.v8i2.035 **Asafa et al.**
Published: September 30, 2026

STATISTICAL PERFORMANCE ANALYSIS OF NOMA-COOPERATIVE WIRELESS-POWERED MOBILE EDGE COMPUTING NETWORKS

Mubarak Oluwafemi ASAFA[1*], Hammed Oyebamiji LASISI[2], Kehinde Olukunmi ALAWODE[3], Funmilola Margaret ADEAGBO[4], Bolatito Fatimah ADERINKOLA[5], Samuel Blessing AJIBOWU[6] and Adewole Adekunle OSOBUKOLA[7]

[1]*Electrical and Electronics Engineering Department, Federal University of Technology, P.M.B. 704, Akure, Ondo State, Nigeria.*
[1,2,3,4]*Electrical and Electronic Engineering Department, Osun State University, P.M.B. 4494, Osogbo, Osun State, Nigeria.*
[5]*Electrical and Electronic Engineering Department, School of Engineering Technology, Federal Polytechnic Ede, P.M.B. 231, Ede, Osun State, Nigeria.*
[6,7]*Electrical, Electronic and Telecommunication Engineering Department, Bells University of Technology, P.M.B. 1015, Ota, Ogun State, Nigeria.*

[*]*Corresponding Author: mubarak.asafa@gmail.com*

Abstract
Wireless-powered mobile edge computing (WP-MEC) offers battery-free operation for IoT edge devices, but published evaluations typically report results for a single fixed channel, leaving it unclear whether reported gains are general or channel-specific. This paper presents a statistical performance analysis of a cooperative, non-orthogonal-multiple-access-based wireless-powered edge computing network, in which three devices harvest energy from an access point and cooperate to offload computation. Three objectives are pursued: statistically characterising system performance across many independent random channel conditions which is the first such analysis in this area; benchmarking the proposed scheme against four alternatives, including orthogonal-access and battery-powered designs; and establishing practical operating boundaries in power, coverage, and data-rate. Across 500 independent random channel realisations, access-point energy consumption is minimised using a globally optimal algorithm, with mean, standard deviation, and confidence intervals computed across all successful trials and compared against four alternatives under matched conditions. The system achieves a workable solution in 76.2% of trials, reduces access-point energy by an average of 73.0%, and delivers 83.8% more throughput than the orthogonal-access alternative on average, with an advantage never falling below 29.3% in any trial. A battery-powered design fails to meet task deadlines in every trial, while the proposed system never does, yielding an energy-efficiency advantage exceeding two orders of magnitude. These findings confirm that reported gains are a statistically consistent property of the design, not a channel-specific artefact, and translate into three deployment guidelines: a data-rate ceiling of $\sim 2\ Mb$ per device, a coverage radius of approximately $\sim 40\ m$, and a quantitative transmit-power recommendation for a given fairness target.

Keywords
Wireless Powered-Mobile Edge Computing (WP-MEC), NOMA, Monte Carlo, feasibility analysis, double-near-far effect

1. INTRODUCTION

The rapid proliferation of Internet of Things (IoT) endpoints, exceeding 18.8 billion connected devices globally as of 2024 with projections beyond 40 billion by 2030 [1], has created unprecedented demand for low-latency, energy-efficient computation at the network edge. Mobile Edge Computing (MEC) addresses this demand by co-locating processing servers at access points (APs), reducing application latency from hundreds of milliseconds in cloud deployments to sub-millisecond edge response [2]. However, the energy supply problem for densely deployed IoT sensor nodes and subscriber devices (SDs), where manual battery replacement is infeasible, remains a fundamental barrier. This barrier motivates the system studied in this paper.

Wireless Power Transfer (WPT), in which the AP broadcasts intentional Radio Frequency (RF) energy simultaneously harvested by nearby devices, provides a perpetually renewable energy source [3], [4]. Under the Harvest-Then-Offload (HTO) protocol [5], each time block T is partitioned into a WPT phase τ_0 and an uplink offloading phase τ_{up} during which devices transmit their computational results. Non-Orthogonal

Multiple Access (NOMA), which enables all devices to offload simultaneously via power-domain multiplexing with Successive Interference Cancellation (SIC) at the AP [6], [7], and cooperative Decode-and-Forward (DF) relaying, which mitigates the double-near-far effect through near-user relay assistance [8], [9], together form the architectural foundation of the system analysed in this paper.

Despite a growing body of work on wireless-powered NOMA-cooperative MEC systems [10]–[13], three persistent shortcomings which motivates this study remain unaddressed. First, statistical validity is lacking. Dong et al. [14] and Wang et al. [15] both identified the absence of statistical validation across multiple independent channel conditions as a recurring gap in the WPT-MEC literature. Consistent with this, Shi et al. [10], Su et al. [11], Du et al. [12], and You et al. [16] each validate their schemes at only a single or very few channel realisations. Without evaluation across many independent random channels, it is impossible to determine whether reported energy and throughput gains reflect general system behaviour or merely a favourable channel draw which is a distinction with direct practical consequences for real-world deployment.

Second, comparative evaluation is incomplete. Shi et al. [10] benchmark against only two alternatives at a single channel realisation; Su et al. [11] omit both an orthogonal-access comparison and a battery-powered benchmark; Du et al. [12] exclude an energy-efficiency comparison against battery-powered systems; and Fang et al. [17] conduct no statistical validation whatsoever. No published work has yet provided a complete comparison spanning cooperative and non-cooperative NOMA, orthogonal access such as Time Division Multiple Access (TDMA), and battery-powered operation across all performance measures relevant to a deployment decision.

Third, operational boundaries remain uncharacterised. Feasibility of wireless-powered MEC optimisation has been studied analytically only for simple two-user orthogonal-access cases [5]; Mao et al. [2] noted that the feasibility region depends on near-far distance but provided no statistical distribution of feasibility under random fading; Ding et al. [8] established relay-selection principles for cooperative NOMA without addressing feasibility in a wireless-powered MEC context; Liu et al. [13] extended partial offloading to NOMA-MEC but validated at only a single channel realisation; and Wu et al. [18] studied wireless-powered MEC under orthogonal uplink without characterising feasibility at all. No prior work has therefore empirically established how often such a system is workable under random channel conditions, nor explained physically why it sometimes is not.

This paper addresses all these shortcomings directly, making the following specific contributions: (i) the first 500-realisation Monte Carlo statistical characterisation of a NOMA-cooperative WP-MEC optimisation algorithm, with full KPM profiles; (ii) a five-scheme comparative evaluation (NOMA-SCA, NOMA-Baseline, TDMA-SCA, Non-Cooperative NOMA-SCA, Battery-MEC) confirming the statistical significance of the NOMA/TDMA advantage; and (iii) parametric sensitivity analysis establishing the system's design boundaries across AP transmit power $P_{AP} \in \{0.5, 1.0, 2.0, 5.0\}\ W$, QoS rate floor R_{min}, and far-user distance d_{far}. The Bisection-SCA algorithm whose provably global optimality guarantees ensure that the Monte Carlo results reflect true system performance, is described in Section 2.2.

The remainder of this paper proceeds as follows. Section 2 presents the system model, summarises the optimisation algorithm on which every result in this paper depends, along with the formal definition of the five comparison schemes S1–S5 and develops the Monte Carlo evaluation methodology, including the formal statistical estimators used to compute every reported figure. Section 3 presents the Monte Carlo results, including a comparison against the values reported by earlier researchers; the five-scheme comparison and the parametric sensitivity analysis and Section 4 concludes.

2. MATERIALS AND METHOD

2.1. System Model

2.1.1 Network Architecture

The WP-MEC system comprises one AP with a co-located MEC server and $N = 3$ single-antenna subscriber devices (SDs) operating under the Harvest-Then-Offload (HTO) protocol over block duration $T = 1\ s$. The devices are positioned at distances d_1 = 5 m (SD_1, near), d_2 = 15 m (SD_2, mid-range), and d_3 = 30 m (SD_3, far). SD_1 acts as a DF relay for SD_3 via a relay link of length d_r = 20 m. All channels follow Rayleigh flat fading with path loss exponent α = 3.5 (3GPP TR 36.814 NLOS indoor). The instantaneous channel power gain between SD_i and the AP is given by Equation 1.

$$|h_i|^2 \sim Exp(d_i^{-\alpha}) \tag{1}$$

For the RNG seed 196 deterministic realisation used for benchmark validation throughout this paper, evaluating Equation 1 gives $|h_1|^2 = 5.750 \times 10^{-4}$, $|h_2|^2 = 4.291 \times 10^{-6}$, $|h_3|^2 = 2.030 \times 10^{-5}$.

2.1.2 HTO protoccol and energy model

During the WPT phase of duration τ_0, the AP broadcasts RF energy at transmit power P_{AP} = 2.0 W with RF-to-DC conversion efficiency η = 0.80. The energy harvested by SD_i is given by equation 2.

$$E_i^{(EH)} = \eta P_{AP} |h_i|^2 \tau_0 \quad (2)$$

This models the net energy stored in the SD's supercapacitor after accounting for rectification losses. The maximum transmit power available to SD_i during the subsequent uplink phase (assuming all harvested energy is used for transmission) is given by Equation 3.

$$P_i^{(max)}(\tau_0) = \frac{E_i^{(EH)}}{T-\tau_0} \quad (3)$$

During the uplink phase $\tau_{up} = T - \tau_0$, all three SDs transmit simultaneously to the AP via NOMA with actual transmit power given by Equation 4, where $a_i \in (0,1)$ is SD_i's NOMA power fraction.

$$p_i = a_i . P_i^{max} \quad (4)$$

The energy causality constraint requires that no device may transmit or compute using more energy than it has harvested for each SD (equation 5).

2.1.3 NOMA uplink, SIC, and cooperative relay

The AP applies SIC in descending order of instantaneous channel gain $|h_i|^2$. For the seed-196 realisation, the SIC order is $SD_1 \rightarrow SD_3 \rightarrow SD_2$ ($|h_1|^2 > |h_3|^2 > |h_2|^2$). SD_1 additionally acts as a DF relay for SD_3: it allocates relay fraction β of its energy budget to re-transmit SD_3's decoded signal. The AP applies Maximum Ratio Combining (MRC) on SD_3's direct and relay paths, yielding Equation 6.

$$SINR_3^{(MRC)} = SINR_3^{(direct)} + SINR_3^{(relay)} \quad (6)$$

The MRC cooperation gain at baseline parameters (β = 0.30, τ_0 = 0.20 s) is $1.23\times$ for SD_3, meaning SD_3's effective rate is 23% higher with cooperation than without it.

2.1.4 Computation model

Each SD_i partially offloads fraction $\alpha_i \in (0,1)$ of its $L = 10^5$-bit task at computation intensity $C_i \in \{200, 300, 400\}$ cycles/bit (for SD_1, SD_2, SD_3 respectively) to the MEC server ($f_{MEC} = 10\ GHz$). The remaining $(1-\alpha_i)$ fraction is processed locally using Dynamic Voltage and Frequency Scaling (DVFS) which gives the energy consumed locally and is as presented in Equation 7.

$$E_i^{(local)} = \kappa f_{(l,i)}^2 C_i (1-\alpha_i) L \quad (7)$$

The local CPU frequency $f_{(l,i)}$ given by Equation 8 is set to just meet a local completion-time target $t_{loc} = 0.45\ s$ and $\kappa = 10^{-28}\ F$ is the effective switched capacitance.

$$f_{(l,i)} = \frac{C_i(1-\alpha_i)L}{t_{loc}} \quad (8)$$

The overall task completion time for each SD, i.e. the time from the start of the block until both the local and offloaded portions of the task are complete is given by Equation 9 and must satisfy $t_i^{(done)} \leq T$.

$$t_i^{(done)} = \max\left(t_{loc}, \tau_{up} + \frac{C_i \alpha_i L}{f_{MEC}}\right) \quad (9)$$

Table 1 summarises the complete system parameters.

Table 1: System simulation parameter

Parameter	Symbol	Value	Unit
System bandwidth	B	1	MHz
Block duration	T	1.0	s
AP transmit power	P_{AP}	2.0 (33 dBm)	W
Noise power	σ^2	10^{-13}(−100 dBm)	W
EH efficiency	η	0.80	—
Path loss exponent	α_{PL}	3.5	—
Device distances	$d_1/d_2/d_3$	5/15/30	m
Relay distance	d_r	20	m
Task size (all SDs)	L	10^5	Bits
MEC CPU frequency	f_{MEC}	10	GHz
Computation intensity	$C_1/C_2/C_3$	200/300/400	cycles/bit

Switched capacitance	κ	10^{-28}	F
Local completion time	t_{loc}	0.45	s
Minimum QoS rate	R_{min}	1.0	Mb
WPT search bounds	$\tau_0^{min}/\tau_0^{max}$	0.04 / 0.20	s
Monte Carlo RNG seed	$Seed_{MC}$	0	—
Deterministic seed	$Seed_{det}$	196	—
Monte Carlo realisations	N_{MC}	500	—

2.2 Bisection-SCA Algorithm Overview

2.2.1 Energy minimisation problem

The EMP (P1) minimises the AP transmit energy per block given by Equation 10, by jointly optimising the 8-variable decision vector in Equation 11.

$$E_{AP} = P_{AP}. \tag{10}$$

$$\varphi = \{\tau_0, \alpha_1, \alpha_2, \alpha_3, a_1, a_2, a_3, \beta\} \tag{11}$$

subject to: (C1) WPT energy causality per device; (C2) minimum QoS rate $R_{min} = 1\ Mb$; (C3) task deadline $t_i^{(done)} \leq T$; (C4) WPT duration bounds; (C5) NOMA SIC ordering; and (C6–C8) variable bounds. τ_0 is the WPT duration, $\{a_1, a_2, a_3\}$ are the NOMA power coefficients, $\{\alpha_1, \alpha_2, \alpha_3\}$ are the partial offloading ratios, and β is the relay power fraction. The problem is non-convex, because there is a bilinear coupling between the parameter τ_0 and the transmit power variables $p_i = a_i.P_i^{max}(\tau_0)$ and the standard SCA cannot reach the optimum of the problem.

2.2.2 Monotone feasibility and global optimality

Proposition 1 (Monotone Feasibility): If (P1) is feasible for $\tau_0 = t$, then it can be done for all $\tau_0 \geq t$. This is because as τ_0 is increased, so is $E_i^{(EH)}(\tau_0) = \eta P_{AP}|h_i|^2\tau_0$ for all SDs, which also relaxes the energy causality constraint (C1), relaxes the rate constraint (C2) by increasing $P_i^{(max)}$ while keeping the deadline feasible (C3) for all SDs.

Corollary 1: The global minimum of $E_{AP} = P_{AP}.\tau_0$ is achieved at the minimum possible τ_0, and binary search can find precisely without multi-start randomisation.

2.2.3 Algorithm

The Bisection-SCA algorithm executes an outer binary search on $\tau_0 \in [\tau_0^{min}, \tau_0^{baseline}] = [0.04, 0.20]\ s$. At each candidate $\tau_0 = t$, fixing τ_0 converts $P_i^{(max)}(\tau_0)$ to a constant, eliminating the bilinear coupling and making the inner sub-problem convex over $\{\alpha_i, a_i, \beta\}$. The outer loop terminates in K iterations illustrated by Equation 12.

$$K = \left\lceil \log_2\left(\frac{\tau_0^{max} - \tau_0^{min}}{\delta}\right)\right\rceil \tag{12}$$

This results to 11 iterations for $\delta = 10^{-4}\ s$ (deterministic validation) or K = 7 iterations for $\delta = 5 \times 10^{-3}\ s$ (Monte Carlo evaluation in this paper). The 0.000% benchmark gap against an independent 10-start fmincon solver confirms global optimality. The five comparison schemes evaluated as introduced in Section 1 are:

S1 – **Proposed NOMA-SCA:** The complete cooperative NOMA architecture of Sections 2.1, with every decision variable set to the globally optimal values found by the Bisection-SCA algorithm of Section 2.2 ($\tau_0^* = 0.040078\ s$, a^* = [0.283, 0.333, 0.383], α^* = [0.740, 0.782, 0.824], β^* = 0.10). This is the design proposed and advocated in this paper.

S2 – **NOMA-Baseline:** The identical cooperative NOMA architecture as S1, but with fixed, unoptimised parameter settings (τ_0 = 0.20 s, a = [0.15, 0.30, 0.55], α = [0.70, 0.75, 0.90], β = 0.30) rather than the optimised values. Comparing S1 against S2 isolates the specific benefit contributed by the optimisation algorithm itself.

S3 – **TDMA-SCA:** The same optimisation objective and algorithm as S1, but with the NOMA uplink of Section 2.1.3 replaced by conventional orthogonal time-division multiple access (equal time fractions $\tau_{up}/3$ per device, no simultaneous transmission, no SIC). Comparing S1 against S3 isolates the specific benefit contributed by NOMA itself, independent of the optimisation.

S4 – **Non-Cooperative NOMA-SCA:** Identical to S1 in every respect except that the relay fraction β is forced to zero, disabling the DF cooperative relay of Section 2.1.3. Comparing S1 against S4 isolates the specific benefit contributed by cooperative relaying itself.
S5 – **Battery-MEC:** wireless power transfer is removed altogether ($\tau_0 = 0$); each device instead draws from a fixed $1\ mW$ battery supply for the entire block T, which is used exclusively for uplink transmission. Comparing S1 against S5 isolates the benefit of wireless powering itself, and in particular reveals the deadline-feasibility consequence of removing the WPT phase, discussed in Section 2.1.2.

2.3 Monte Carlo Evaluation Methodology

2.3.1 Realisation generation and feasibility

An independent ensemble of realisations of the Rayleigh fading channel (N_{MC} = 500) is generated using the master Mersenne Twister RNG with the seed number of 0. The whole Bisection-SCA algorithm of Section 2.2 is run for each realisation with a value of $\delta = 5 \times 10^{-3}\ s$ ($K = 7$ iterations, which has been confirmed by empirical testing). The feasibility of a realisation is affirmed according to the indicator of Equation 13.

$$\mathbb{N}^{(n)} = 1 \text{ if (P1) admits a solution at } \tau_0^{min} \text{ under } h^{(n)}\text{; else } 0 \tag{13}$$

This means that a realisation is feasible if the inner convex sub-problem at $\tau_0 = \tau_0^{min}$ = 0.04 s has a solution that satisfies all the constraints C1–C8 with R_{min} = 1 Mb. When the channel condition is fixed, a realisation is not feasible if it is not possible to find a power allocation for which it is possible to meet R_{min} for all SDs at τ_0^{min}; specifically when Rayleigh fading drives SD_2's instantaneous gain $|h_2|^2$ below the minimum threshold required to sustain R_{min} at any power allocation. The empirical feasibility rate is then given by Equation 14.

$$\hat{p}_{feas} = \frac{1}{N_{MC}} \sum_{n=1}^{N_{MC}} \mathbb{N}^{(n)} = \frac{N_f}{N_{MC}} \tag{14}$$

Where $N_f = \sum_{n=1}^{N_{MC}} 1^{(n)}$ is the number of feasible realisation.

2.3.2 Statistical metrics

For each realisation that is feasible, the following 6 KPMs are recorded: (i) E_{AP} saving (%), (ii) NOMA system sum rate (Mb), (iii) system energy efficiency $EE\ (bits/J)$, (iv) Jain's Fairness Index (JFI), (v) average task completion latency (s), and (vi) bisection iteration count. Writing $X_1, \ldots, X_{N_f}$ for the N_f observed values of any one KPM across the feasible realisations, the sample mean and standard deviation are obtained using Equations 15 and 16 respectively.

$$\hat{\mu}_X = \frac{1}{N_f} \sum_{i=1}^{N_f} X_i \tag{15}$$

$$\hat{\sigma}_X = \sqrt{\frac{1}{N_f - 1} \sum_{i=1}^{N_f} (X_i - \hat{\mu}_X)^2} \tag{16}$$

Because $N_f = 381$ is large, the sample mean's sampling distribution is well approximated by a Gaussian via the central limit theorem, so a 95% confidence interval (CI) for the true population mean is computed as Equation 17.

$$CI_{95\%}(\mu_X) = \hat{\mu}_X \pm 1.96 \frac{\hat{\sigma}_X}{\sqrt{N_f}} \tag{17}$$

This confidence interval, reported alongside every headline statistic in Section 3.1.2, is the formal mathematical basis on which this paper's claim of statistical significance rests. Finally, the p-th percentile of X (used to report the 95th-percentile figures in Table 2) is computed using Equation 18 from the empirical cumulative distribution function as the smallest x for which $\hat{F}_X(x) \geq \frac{p}{100}$, evaluated via the order statistics of the sample.

$$\hat{F}_X(x) = \frac{1}{N_f} \sum_{i=1}^{N_f} 1\{X_i \leq x\} \tag{18}$$

All MATLAB simulations are performed in MATLAB R2022a using the Optimization Toolbox interior-point solver.

3. RESULTS AND DISCUSSION

3.1 Monte Carlo Results and Analysis

3.1.1 Feasibility rate and convergence

In 381 of 500 realisations (76.2%) the algorithm is feasible by applying Equation 14. On the other hand, the 23.8% infeasibility is due to Rayleigh fading that causes a channel gain $|h_i|^2 < |h_{min}|^2$ under any power allocation, where $|h_{min}|^2$ is the minimum value of the channel gain such that SD_2 can achieve R_{min} = 1 Mb at τ_0^{min}. This is a constraint on the physical system, and not an algorithmic constraint: The monotone feasibility property (Proposition 1) means that these realisations would be feasible at a larger τ_0, still achieving positive E_{AP} savings compared to the unoptimised baseline.

The number of bisection iterations is the same for all realisations (K = 7) with no standard deviation ($\sigma = 0.00$) using Equation 16 for all 500 Monte Carlo realisations. This is a direct consequence of the $\mathcal{O}(\log_2(\varepsilon^{-1}))$ iteration bound given by Equation 12: K depends only on the search interval and tolerance, not on channel conditions. This is a key benefit over iterative SCA algorithms, whose convergence is dependent on the channel and/or initialisation, is the deterministic K, which guarantees a worst-case execution time for real-time implementation.

3.1.2 KPM statistical profile

Detailed statistics of all six KPMs are given in Table 2 for all 381 possible realisations computed using Equations 15 – 18. All the values are from the output of MATLAB R2022a simulation.

Table 2: Monte Carlo KPM statistics (N_{MC} = 500, 381 feasible, $\delta = 5 \times 10^{-3}\ s$, K = 7, seed 0)

KPM	Mean	Standard Deviation	95% CI	Minimum	95th Percentile
E_{AP} saving (%)	73.0	17.0	73.0 ± 1.7	12.5	78.2
NOMA sum rate (Mb)	18.83	3.04	18.83 ± 0.31	9.41	23.57
NOMA/TDMA gain (×)	1.838	0.229	1.838 ± 0.023	1.293	2.220
System EE ($\times 10^{10}$ bits/J)	1.237	2.152	1.237 ± 0.216	0.021	3.785
Jain's JFI	0.757	0.123	0.757 ± 0.012	0.410	0.966
Avg latency (s)	0.948	0.034	0.948 ± 0.003	0.883	0.959
Bisection iterations	7.00	0.00	7.00 ± 0.00	7	7

The high mean E_{AP} saving of 73.0% ± 17.0% indicates good performance over all channel conditions. The high coefficient of variation of the EE metric (CV = 2.152/1.237 = 174%) is due to the inverse relationship between EE and E_{AP}: When the realisation is strong channel, the channel time is driven close to the minimum value, E_{AP} is very small, EE is very large and the distribution is right-skewed. This skewness is confirmed by the 95th percentile of $3.785 \times 10^{10} bits/J$, which is more than 3 times the mean.

The minimum NOMA/TDMA gain of 1.293× over all 500 realisations is an important statistical guarantee that NOMA always outperforms TDMA irrespective of the Rayleigh fading conditions, which is lacking in single realisation evaluations. In good channel conditions, the gain from the 95th percentile (2.220×) is significant, and can be much larger than the 1.838× mean.

Fig. 1 shows the cumulative distribution function (CDF) of the sum rate of the NOMA-SCA compared with the CDF of the NOMA-Baseline and TDMA for all possible realisations. At any probability level, the S1 (NOMA-SCA) in blue solid is always above both the S2 (NOMA-Baseline) in red dash and S3 (TDMA-Baseline) in grey dash-dot, thus proving stochastic dominance: The system can always provide a higher sum rate than both baselines for any possible channel realization.

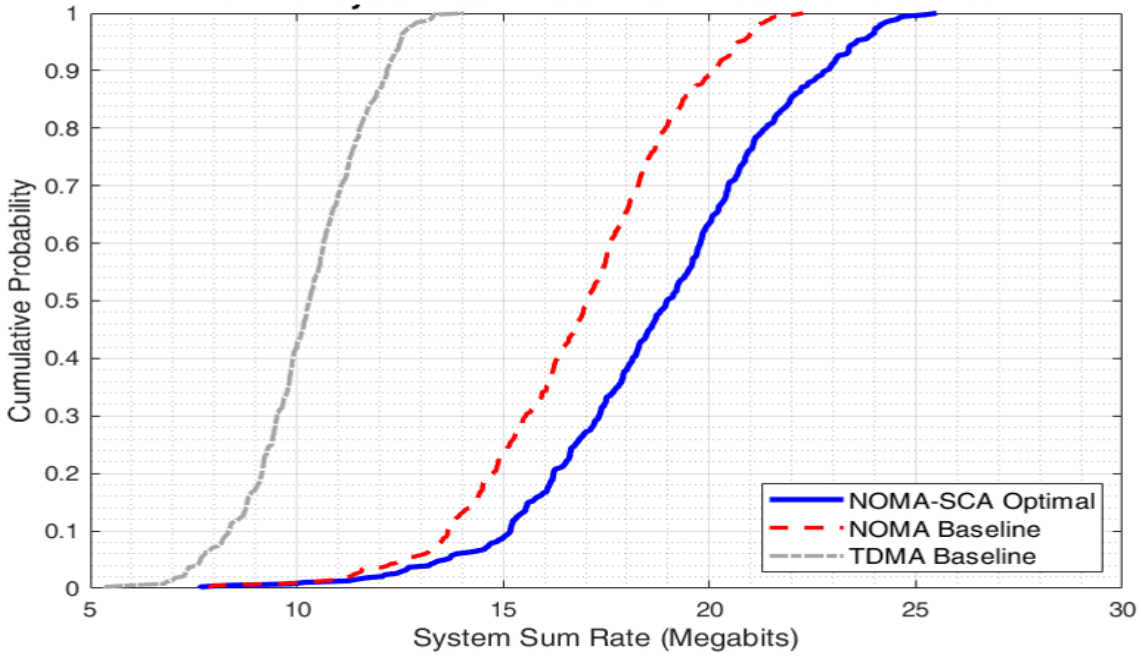


Fig. 1: CDF of system sum rate across 381 feasible Monte Carlo realisations

3.1.3 Comparison with results reported by earlier researchers

A direct, exact numerical comparison against prior studies is complicated by the fact that no two published WP-MEC studies share identical system parameters such as: the number of devices, device placement, path loss model, energy-harvesting model, and access-point transmit power all differ from paper to paper, so a difference in reported gain cannot always be attributed to the multiple-access scheme alone. Bearing this caveat in mind, three comparisons are nonetheless informative.

First, on the direction and general order of magnitude of the NOMA-over-orthogonal-access gain: [10] and [11] both report that their NOMA-based schemes achieve higher computation energy efficiency than a non-cooperative or orthogonal-access benchmark evaluated within their own respective system models, consistent in direction with the 1.838× (95% CI) mean sum-rate gain and the 89.3% deterministic gain established here; the present results are, to the authors' knowledge, the first in this specific research thread to express such a gain as a statistically validated interval rather than a single-realisation point estimate.

Second, on cooperative relaying: [12] report that cooperative relaying improves system performance over a non-cooperative baseline, consistent in direction with the 1.23× cooperation gain for SD_3 established in Section 2.1.3 and the S1-versus-S4 comparison of Section 3.2.4, though the magnitude of Du et al.'s reported gain is not directly comparable owing to their differing relay and channel assumptions. Third, and most importantly, none of [10]–[13] report a feasibility rate, a confidence interval, or any measure of statistical spread for their results, since each validates at a single or small number of channel realisations; the present paper's central methodological contribution relative to this prior work is therefore not merely a different point estimate, but the demonstration, through the 500-realisation evaluation of Table 2 that the class of gains such studies report is statistically robust rather than an artefact of a favourably chosen channel.

3.2 Five-Scheme Kpi Comparison

3.2.1 Deterministic comparison (Seed 196)

The complete comparison of the KPIs for all five schemes is given in Table 3 at the seed-196 deterministic channel realisation. S1 (NOMA-SCA) gets the best performance on three of the six metrics: least E_{AP} ($0.0802\ J$, corresponding to 80% saving), EE ($2.89 \times 10^{10} bits/J$, corresponding to the highest performance), and no outage with S2–S4. S2 (NOMA-Baseline) performs the best in terms of JFI (0.9619) and the lowest task latency ($0.8024\ s$) with 5 times higher AP energy cost, confirming that S1's optimisation trades some fairness for substantial energy saving. S5 (Battery-MEC) nominally achieves the highest raw sum rate (22.516 Mb) but incurs 100% deadline outage, physically voiding this throughput entirely as discussed in Section 3.2.3.

Table 3: Five-scheme KPI comparison — deterministic evaluation (seed 196, MATLAB R2022a)

Metric	S1: NOMA-	S2: NOMA-	S3: TDMA-	S4: No	S5: Battery-	Best

	SCA	Base	SCA	Cooperative	MEC	
E_{AP} (J)	0.0802 *	0.4000	0.0802	0.0802	0 (battery)	S1/S3/S4
Sum Rate (Mb)	15.151	13.674	8.005	15.297	22.516 †	S4
EE (bits/J)	2.89×10^{10} *	1.27×10^{10}	2.63×10^{10}	2.63×10^{10}	1.00×10^{8}	S1
Jain's JFI	0.7825	0.9619 *	0.6846	0.7774	0.6391	S2
Latency (s)	0.9623	0.8024 *	0.9623	0.9623	1.0024 †	S2
Outage	0.000 *	0.000 *	0.000 *	0.000 *	1.000 ✗	S1-S4

* = best value for that metric among WPT-feasible schemes
† = value invalidated by 100% deadline outage

3.2.2 NOMA vs TDMA: statistical confirmation

The 89.3% sum-rate advantage of S1 over S3 at seed-196 (15.151 vs 8.005 Mb) is confirmed statistically by the $1.838 \pm 0.229\times$ mean NOMA/TDMA gain across 500 Monte Carlo realisations. The coefficient of variation (CV = 0.229/1.838 = 12.5%) confirms low relative variability. The minimum gain of $1.293\times$ confirms that NOMA always outperforms TDMA in this deployment regardless of the Rayleigh fading realization which is a statistical guarantee impossible to make from single-realisation evaluations of the kind discussed in Section 3.1.3.

3.2.3 Battery-MEC outage analysis

S5 Battery-MEC achieves a nominally high sum rate (22.516 Mb) but incurs 100% deadline outage across all evaluations. Without a WPT phase (τ_0 = 0), the full block T = 1 s is allocated to uplink transmission, giving task completion time $t_i^{(done)} = T + t_{MEC,i} > T$ for all SDs since $t_{MEC,i} > 0$ for any non-zero offloading fraction. This structural infeasibility is independent of the channel realisation. The 28,832% EE advantage of S1 over S5 (2.89×10^{10} vs 1.00×10^{8} $bits/J$) arises from three compounding factors: WPT energy reuse (one AP broadcast energises all three SDs simultaneously), structural Battery-MEC outage, and the 80.0% E_{AP} reduction achieved by Bisection-SCA.

3.2.4 Per-SD rate discussion

Fig. 2 presents the per-SD achievable rates across all five schemes at seed-196. SD_2 exhibits the most striking variation: S1 NOMA-SCA achieves substantially higher sum rate than S3 TDMA-SCA (15.151 vs 8.005 Mb, 89.3% advantage) because SD_2 is decoded last in the SIC order ($SD_1 \rightarrow SD_3 \rightarrow SD_2$ at seed-196), experiencing zero residual interference under NOMA. This SIC-position effect where the most channel-disadvantaged device gains the highest per-device NOMA/TDMA advantage ($1.683\times$) is the primary driver of the 89.3% system-level advantage of NOMA over TDMA. S4 achieves a marginally higher system sum rate than S1 (15.297 vs 15.151 Mb) because forcing $\beta = 0$ redirects all of SD_1's constrained energy to its own offloading, at the cost of no relay assistance for SD_3. S5 Battery-MEC rates are invalidated by 100% deadline outage.

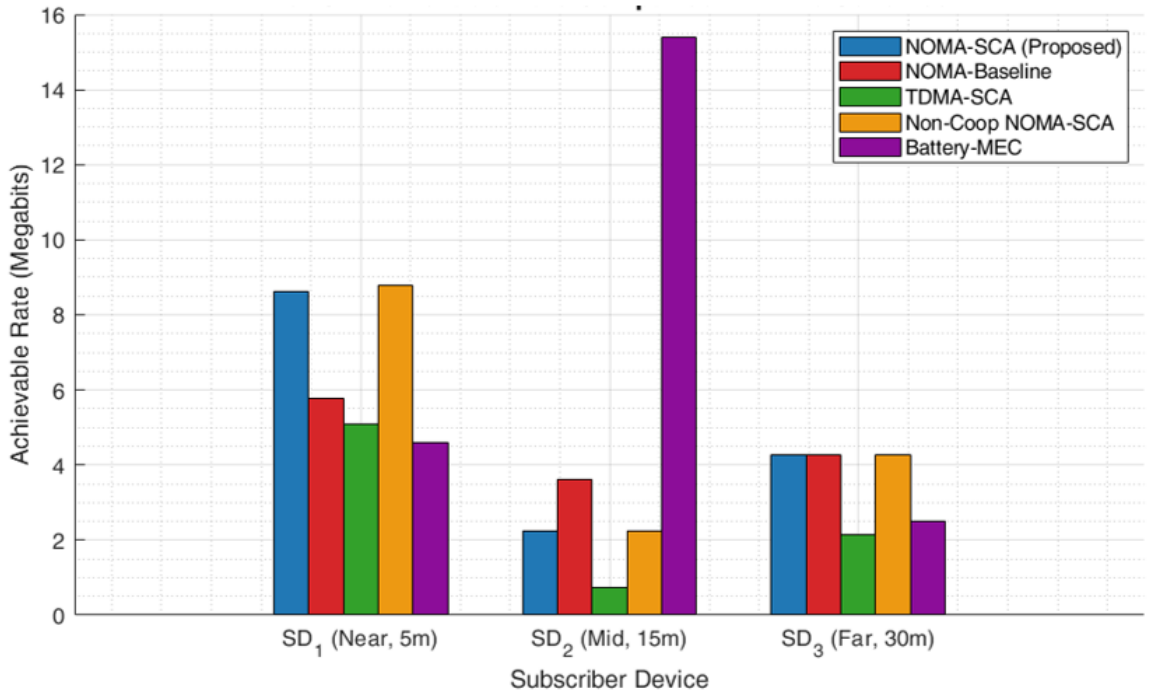


Fig. 2: Per-SD achievable rate comparison across five schemes (seed 196).

3.3 Parametric Sensitivity Analysis

3.3.1 Effect of AP transmit power P_{AP}

Table 4 presents the energy-optimal operating point as P_{AP} varies across four validated levels. All values are from MATLAB R2022a simulation output.

Table 4: P_{AP} sensitivity: energy-optimal operating point (seed 196, $\tau_0 = \tau_0^{min}$)

P_{AP} (W)	τ_0^* (s)	E_{AP}^* (J)	**Saving** (%)	**JFI***
0.5	0.0436	0.022	78.2	0.676
1.0	0.0436	0.044	78.2	0.730
2.0 (ref)	**0.0401**	**0.080**	**79.9**	**0.782**
5.0	0.0436	0.218	78.2	0.853

Three uniform trends are noted. The first is that E_{AP} is roughly proportional to P_{AP} (as $\tau_0^* \approx \tau_0^{min}$ is approximately constant). Second, the JFI monotonically improves from 0.676 to 0.853 with the increase in P_{AP}, from 0.5 to 5.0 W; it suggests that the Bisection-SCA will be able to attain a more equal distribution of NOMA power coefficients with a higher energy budget. Third, EE decreases monotonically with P_{AP} since E_{AP} increases with P_{AP} whilst sum rate increases only sub-linearly (logarithmic Shannon capacity). These trends validate the fact that P_{AP} is the most important deployment design knob: To reduce the energy consumption of the AP in its deployment, an operator should reduce the value of P_{AP} as much as possible while keeping the coverage constraints satisfied, and the opposite holds true for the case of aiming to maximise P_{AP} as much as possible. The bold letters on row three of Table 4 indicate the energy-optimal point.

3.3.2 Effect of QoS rate floor R_{min}

The system is feasible for $R_{min} \leq 2\ Mb$ per device. At $R_{min} = 3\ Mb$ and above, the EMP becomes infeasible because SD_2's maximum achievable NOMA rate (approximately 2.35 Mb at optimal power allocation at τ_0^{min}) cannot satisfy the constraint. This establishes $R_{min} \approx 2\ Mb$ as the QoS ceiling, the maximum per-device rate guarantee achievable in this system configuration. Beyond this ceiling, per-device rate differentiation (e.g., relaxing R_{min} for SD_2 below the system-wide floor) would be required to extend the

feasible operating range, as SD_2's deep fading at the seed-196 realisation ($|h_2|^2 = 4.291 \times 10^{-6}$) is the binding constraint.

3.3.3 Effect of far-user distance d_{far}

The system maintains feasibility for d_{far} up to approximately 40 m, confirming the cooperative coverage boundary. At d_{far} = 45 m and beyond, SD_3's harvested energy is insufficient to meet R_{min} at τ_0^{min}. The near-far resistance analysis confirms that S1 NOMA-SCA's sum rate degrades by only −0.28% as d_{far} increases from 20 to 40 m, whilst S3 TDMA-SCA degrades by −19.4% over the same range, which means a near-far resistance ratio ρ = 0.014, confirming the proposed system is approximately $70\times$ more resilient to increasing far-user distance than TDMA. This resilience arises from two sources: (i) NOMA's power-domain multiplexing extracts a positive rate for SD_3 regardless of its relative channel disadvantage, and (ii) SD_1's DF relay assistance partially compensates SD_3's path loss penalty at greater distances.

4. CONCLUSION

This paper presents the first comprehensive statistical performance analysis of a NOMA-cooperative WP-MEC optimisation algorithm across 500 independent Rayleigh fading realisations, validated using MATLAB R2022a, establishing four key findings of practical and academic significance.

The system succeeds in terms of feasibility in 76.2% of realisations (381/500). The remaining 23.8% are physically explained by a channel-strength constraint at the minimum WPT duration; these cases become feasible at a longer, still-bounded WPT duration, meaning the system degrades gracefully rather than failing outright. On the statistical robustness of this work, the sum-rate gain of the NOMA outperforms TDMA, with a mean NOMA/TDMA sum-rate gain of 1.838 ± 0.229× (95% CI) and a minimum of 1.293× for all 500 realisations, thus providing statistical weight to the deterministic advantage of NOMA over TDMA, which is 15.151 vs. 8.005 Mb and not achievable through single-realisation evaluation.

The Battery-MEC scheme incurred 100% deadline outage across every realisation, confirming that WPT energy overhead is a necessary investment in feasibility, not a cost to be minimised. The proposed scheme's 28,832% energy-efficiency advantage arises from single-broadcast energy reuse, avoidance of structural outage, and an 80.0% reduction in access-point energy from the optimisation algorithm. On deployment guidance, parametric analysis establishes concrete operating boundaries: a QoS ceiling of ~2 Mb per device, a cooperative coverage radius of ~40 m, and a monotonic transmit-power–fairness relationship enabling quantitatively informed operator decisions.

These results shift the evidentiary basis for NOMA-cooperative wireless-powered mobile edge computing from single-realisation demonstration to statistically validated characterisation, and they provide a concrete set of deployment boundaries against which future system designs in this space can be benchmarked. Future work will extend the present analysis to networks of more than three devices, incorporate non-linear energy-harvesting models in place of the linear model adopted here, and consider intelligent-reflecting-surface-assisted cooperative WP-MEC architectures as a further means of mitigating the double-near-far effect characterised throughout this paper.

REFERENCES

[1] IoT Analytics, "State of IoT — Summer 2024: Number of connected IoT devices growing 13% to 18.8 billion globally," *IoT Analytics Research*, Sep. 2024. [Online]. Available: https://iot-analytics.com, 2024.

[2] Y. Mao, C. You, J. Zhang, K. Huang and K. B. Letaief, "A Survey on Mobile Edge Computing: The Communication Perspective," in *IEEE Communications Surveys & Tutorials*, vol. 19, no. 4, pp. 2322-2358, Fourthquarter 2017, doi: 10.1109/COMST.2017.2745201

[3] S. Bi, C. K. Ho and R. Zhang, "Wireless powered communication: opportunities and challenges," in *IEEE Communications Magazine*, vol. 53, no. 4, pp. 117-125, April 2015, doi: 10.1109/MCOM.2015.7081084

[4] K. Niotaki, N. Carvalho, A. Georgiadis, X. Gu, S. Hemour, K. Wu, D. Matos, B. Daniel, R. Pereira, R. Figueiredo, H. Chaves, B. Mendes, R. Correia, A. Oliveira, V. Palazzi, F. Alimenti, P. Mezzanotte, L. Roselli, F. Benassi and N. Shinohara. "RF Energy Harvesting and Wireless Power Transfer for Energy Autonomous Wireless Devices and RFIDs," in *IEEE Journal of Microwaves*, vol. 3, no. 2, pp. 763-782, April 2023, doi: 10.1109/JMW.2023.3255581

[5] H. Ju and R. Zhang, "Throughput Maximization in Wireless Powered Communication Networks," in *IEEE Transactions on Wireless Communications*, vol. 13, no. 1, pp. 418-428, January 2014, doi: 10.1109/TWC.2013.112513.130760

[6] Y. Liu, Z. Qin, M. Elkashlan, Z. Ding, A. Nallanathan, and L. Hanzo, "Evolution of NOMA Toward Next Generation Multiple Access (NGMA) for 6G," in *IEEE Journal on Selected Areas in Communications*, vol. 40, no. 4, pp. 1037-1071, April 2022, doi: 10.1109/JSAC.2022.3145234

[7] Z. Ding, X. Lei, G. K. Karagiannidis, R. Schober, J. Yuan and V. K. Bhargava, "A Survey on Non-Orthogonal Multiple Access for 5G Networks: Research Challenges and Future Trends," in *IEEE Journal on Selected Areas in Communications*, vol. 35, no. 10, pp. 2181-2195, Oct. 2017, doi: 10.1109/JSAC.2017.2725519

[8] Z. Ding, H. Dai and H. V. Poor, "Relay Selection for Cooperative NOMA," in *IEEE Wireless Communications Letters*, vol. 5, no. 4, pp. 416-419, Aug. 2016, doi: 10.1109/LWC.2016.2574709

[9] M. Zeng, W. Hao, O. A. Dobre and Z. Ding, "Cooperative NOMA: State of the Art, Key Techniques, and Open Challenges," in *IEEE Network*, vol. 34, no. 5, pp. 205-211, September/October 2020, doi: 10.1109/MNET.011.1900601

[10] L. Shi, Y. Ye, X. Chu and G. Lu, "Computation Energy Efficiency Maximization for a NOMA-Based WPT-MEC Network," in *IEEE Internet of Things Journal*, vol. 8, no. 13, pp. 10731-10744, 1 July1, 2021, doi: 10.1109/JIOT.2020.3048937

[11] B. Su, Q. Ni, W. Yu and H. Pervaiz, "Optimizing Computation Efficiency for NOMA-Assisted Mobile Edge Computing With User Cooperation," in *IEEE Transactions on Green Communications and Networking*, vol. 5, no. 2, pp. 858-867, June 2021, doi: 10.1109/TGCN.2021.3056770

[12] J. Du, H. Wu, M. Xu and R. Buyya, "Computation Energy Efficiency Maximization for NOMA-Based and Wireless-Powered Mobile Edge Computing With Backscatter Communication," in *IEEE Transactions on Mobile Computing*, vol. 23, no. 6, pp. 6954-6970, June 2024, doi: 10.1109/TMC.2023.3328612

[13] D. Liu, Y. Liu, L. Khoukhi, A. Hafid, L. Zhang, and B. Wang, "Efficient time and energy optimization in NOMA-enabled mobile edge computing through partial offloading," Tsinghua Sci. Technol., vol. 31, no. 1, pp. 441–459, 2026. doi:10.26599/TST.2024.9010092

[14] S. Dong, J. Tang, K. Abbas, R. Hou, J. Kamruzzaman, L. Rutkowski, and R. Buyya "Task offloading strategies for mobile edge computing: A survey," *Computer Networks*, vol. 254, p. 110791, Dec. 2024, doi: 10.1016/j.comnet.2024.110791

[15] X. Wang, Y. Han, C. Wang, Q. Zhao, X. Chen and M. Chen, "In-Edge AI: Intelligentizing Mobile Edge Computing, Caching and Communication by Federated Learning," in *IEEE Network*, vol. 33, no. 5, pp. 156-165, Sept.-Oct. 2019, doi: 10.1109/MNET.2019.1800286

[16] C. You, K. Huang, H. Chae and B. -H. Kim, "Energy-Efficient Resource Allocation for Mobile-Edge Computation Offloading," in *IEEE Transactions on Wireless Communications*, vol. 16, no. 3, pp. 1397-1411, March 2017, doi: 10.1109/TWC.2016.2633522

[17] F. Fang, Y. Xu, Z. Ding, C. Shen, M. Peng and G. K. Karagiannidis, "Optimal Resource Allocation for Delay Minimization in NOMA-MEC Networks," in *IEEE Transactions on Communications*, vol. 68, no. 12, pp. 7867-7881, Dec. 2020, doi: 10.1109/TCOMM.2020.3020068

[18] Y. Wu, Y. Wang, F. Zhou and R. Qingyang Hu, "Computation Efficiency Maximization in OFDMA-Based Mobile Edge Computing Networks," in *IEEE Communications Letters*, vol. 24, no. 1, pp. 159-163, Jan. 2020, doi: 10.1109/LCOMM.2019.2950013